Catalysis Science & Technology

Accepted Manuscript

ROYAL SOCIETY OF CHEMISTRY

www.rsc.org/catalysis

Enhanced performance in NO reduction by NH_3 over mesoporous Ce-Ti-MoO_x catalyst stabilized by carbon template

Qiulin Zhang · Xin Liu · Ping Ning* · Zhongxian Song · Hao Li · Junjie Gu

Faculty of Environmental Science and Engineering, Kunming University of Science and Technology. Kunming, 650500, P.R. China.

** Corresponding author. Tel:+ 86-871-65170905.*
E-mail address: ningping_58@126.com

Abstract: Mesoporous Ce-Ti-MoO_x catalysts have been prepared by stabilization with in-situ formed carbon template and used for selective catalytic reduction of NO with NH_3 (NH_3-SCR). The Ce-Ti-MoO_x catalysts were characterized by N_2 adsorption-desorption, XRD, HR-TEM, H_2-TPR and XPS analysis. It was found that the stabilization with carbon template obviously improved the NO conversion of the Ce-Ti-MoO_x catalyst and the pore distribution. The Ce-Ti-MoO_x catalyst stabilization with carbon template at 850 °C in N_2 exhibits the best NH_3-SCR activity and shows uniform mesoporous distribution, and more than 90 % NO conversions were obtained at 175-425 °C with GHSV of 60 000 h^{-1}. The high stabilization temperature with carbon template in N_2 not only leaded to the increase of the specific surface area, the pore volume and low-temperature SCR activity, but also contributed to the enhanced redox properties, the highly dispersed titanium or molybdenum species and the narrow mesoporous distribution. The Ce-Ti-MoO_x with high calcination temperature for removal of carbon template leaded to a drastic decrease of surface area, abrupt decrease of surface oxygen and cerium, produce of rutile TiO_2, and correspondingly low SCR activity.

Key words: Ce-Ti-MoO_x catalyst; Low-temperature NH_3-SCR; Carbon template; Stabilization temperature; Mesoporous

1 Introduction

Ammonia or urea selective catalytic reduction (SCR) is considered as the most effective technology for removal of NO_x from diesel exhaust gases. Vanadium-based catalysts (V_2O_5/TiO_2 promoted by WO_3 or MoO_3) as the most popular commercial catalysts have achieved industrial success for heavy-duty diesel exhausts for years.[1] However, the problems such as, narrow working window (300-400 °C),[2] facile volatility, toxicology of vanadium species in life cycle and the difficulty of disposal the disused catalyst may be an obstacles for further application of the vanadium-based catalysts.[3] Cu or Fe exchanged zeolites with uniform micro-mesorporous and ultra-large surface area have been regarded as the new generation SCR catalysts and have attracted much attention for abatement of NO_x from diesel engine exhaust. However, the expensive price, high consumption of power in producing of zeolites and its inferior SCR activity at low temperature are still the problems for its widely application in practical process.[4] Since typical diesel exhaust temperature downstream the diesel oxidation catalyst (DOC) ranging from 150 to 250 °C for light duty and 200 to 350 °C for heavy duty diesel engines or even lower for an advanced high-efficiency diesel engines.[5, 6] To meet ever-tightening emission regulations, great challenges such as low-temperature activity and working windows remain for De-NO_x catalyst.

Recently, many efforts are focusing on the developing of a cheap and environmental-friendly catalyst with excellent low-temperature SCR activity. Some transitional metal oxide catalysts have been found low-cost and active in NH_3-SCR process.[7-20] It is well known that the basic on NH_3-SCR catalysts in oxygen-rich conditions is standard NH_3-SCR ($4NH_3 + 4NO + O_2 \rightarrow 4N_2 + 4H_2O$) since NO consists > 90% of NO_x in diesel exhausts,[9] while excellent oxygen storage capability (OSC) of CeO_2 could promote the standard NH_3-SCR activity, due to the enhanced activation of chemisorbed NH_3 and shift of NO to NO_2.[10] Anatase TiO_2 with high specific area and excellent sulfur resistance is acclaimed as an ideal carrier for NH_3-SCR process.[3] WO_3 and MoO_3 as "structural" and "chemical" promoters can facilitate NH_3 adsorption during NH_3-SCR process.[10, 11] Compared with WO_3 in commercial SCR catalyst, MoO_3 exhibits a promising advantage of low price.[12]

Ceria-based oxides catalysts with advantages of the unique oxygen storage capacity, excellent redox properties and good sulfur-resistance in NH_3-SCR process have been attracting more attention.[13-20] CeO_2-TiO_2 catalyst has been proved active for NH_3-SCR process, even in the presence of H_2O, CO_2 and C_3H_6.[13, 14] It is reported that the introduction of cerium oxides into titanium-based solid acid catalysts can obviously enhance the SCR activity.[15, 16] In addition, The CeO_2-containing solid acid catalysts also show remarkable NO conversion.[17, 18] Recently, CeO_2-MoO_3 and CeO_2-WO_3 catalyst has been proved to be a promising SCR catalyst for abating diesel exhaust.[19-21] Liu et al. reported that the CeO_2/TiO_2 catalyst doped by MoO_3 exhibited excellent NH_3-SCR activity.[22, 23]

The none-silica materials with uniform mesoporous distribution have been regarded as potential candidates for NH_3-SCR process.[24] However, as far as we know, rare studies have reported for the preparation of tri-metal oxides NH_3-SCR catalysts with uniform mesoporous distribution and large surface area. Luo [25] and Chen [26] et al reported that catalysts with ultra-small particle size, large surface area and porous structures could be prepared by using of carbon template, sintering of the catalysts could be inhibited as well. Compared to various soft or hard template methods, the in-situ formation of carbon template has advantages such as cost-effective preparation and high yield of catalyst. Thus, the present works have attempted to prepare the mesoporous Ce-Ti-MoO_x catalyst stabilization with in-situ formed carbon template by the modified sol-gel method. The influences of the stabilization temperature in the presence of carbon template and the calcination temperature for removal of carbon template on the NH_3-SCR properties have been studied. XRD, XPS, HR-TEM, H_2-TPR and N_2 adsorption-desorption are implemented to characterize structural and chemical promotion properties of the Ce-Ti-MoO_x catalysts.

2 Experimental

2.1 Preparation of the Ce-Ti-MoO_x catalysts

Mo-Ce-Ti-O_x catalysts with Ce/Ti molar ratio of 1:1, nominal MoO_3 content of 10 %, were prepared by a modified sol-gel method. Cerium nitrate, ammonium

molybdate and citric acid were dissolved in the mixture of distilled water and ethanol. Butyl titanate was dissolved in ethanol. The two kinds of solutions were mixed with stirring and then evaporated to form homogenous gels, the gels were subsequently calcined in N_2 atmosphere for 4 h at different temperature for in-situ formation of carbon template, and then the resulting material was calcined in air for 3 h at different temperature for removal of carbon species. Pure MoO_3 was prepared by calcining the ammonium molybdate at 600 °C for 3 h in air. Pure CeO_2 and anatase TiO_2 are purchased from Aladdin Industrial Corporation. The Ce-Ti-MoO_x catalysts were denoted as NxAy, Nx and Ay represents the calcination temperature (x) in N_2 atmosphere and the calcination temperature (y) in air, respectively.

2.2 NH_3-SCR catalytic test

The NH_3-SCR catalytic activity measurement was carried out in a fixed-bed quartz flow reactor (i.d.10mm). The reaction temperature was monitored by a K-type thermocouple inserted into the catalyst bed. Reactant gases were controlled by means of mass-flow controllers before entering reactor. The concentration of simulated gases was as follow: 600 ppm NO, 600 ppm NH_3, 5% O_2, N_2 balanced, the gas hourly space velocity (GHSV) = 60000 h^{-1}. The concentrations of NO and NO_2 in the inlet and outlet gas were continually analyzed by a *RBR Ecome J2KN* flue gas analyzer. The products were analyzed using gas chromatograph (Fuli, 9790) equipment with electron capture detector for N_2O. The NO_x conversion and the N_2 Selectivity were determined by the following equation:

$$NO\ conversion = \frac{NO_x(inlet) - NO_x(outlet)}{NO_x(inlet)} \times 100\% \quad (1)$$

$$S_{N_2} = \frac{NO_x(inlet) - NO_x(outlet) - 2N_2O(out)}{NO_x(inlet) - NO_x(outlet)} \times 100\% \quad (2)$$

Where NO_x (inlet) represents the NO_x concentrations in the feed stream, N_2O(out) and NO_x (outlet) represent N_2O and NO_x concentrations in the effluent gases, respectively. S_{N_2} represents the N_2 selectivity.

2.3 Characterization of the catalysts

The X-ray diffraction (XRD) patterns were recorded on a Bruker D-8 Advance diffractometer operating at 40 kV and 40 mA with Cu Kα radiation (λ = 0.15406 nm) at a rate of 5°/min. Specific surface areas (*SSA*) were determined by nitrogen adsorption-desorption at 77 K on a TriStar II 3020 instrument. The pore volume and pore volume distribution was determined by the adsorption isotherms. The X-ray photoelectron spectroscopy (XPS) studies were carried out on a ULVAC PHI 5000 Versa Probe-□equipment with Al Kα X-ray radiation under UHV. All peaks are calibrated by the C1s peak (284.8 eV). The high-resolution transmission electron microscopy (HR-TEM) characterizations were performed on a FEI Tecnai G220 apparatus operating at 200 kV. The H_2-temperature programmed reduction (H_2-TPR) was carried out in a quartz reactor, and a 100 mg of sample was first pre-treated in N_2 (30 mL·min^{-1}) at 400 °C and cooled to room temperature. After that, a flowing mixture of 5% H_2/Ar (30 ml· min^{-1}) was switched on with a linear heating rate of 8 °C · min^{-1}. The H_2 consumption signal was continuously monitored by a thermal conductivity detector (TCD).

3. Results and discussion

3.1 NH_3-SCR catalytic activity

The effects of the stabilization temperature in the presence of carbon template and the calcination temperature for removal of carbon template on the NH_3-SCR properties have been studied for the Ce-Ti-MoO_x catalyst. As shown in **Fig. 1(a)**, the Ce-Ti-MoO_x catalyst with different stabilization temperatures in the presence of carbon template in N_2 atmosphere shows a vary activity for the reduction of NO by NH_3. It can be seen that increasing stabilization temperature in the presence of carbon template in N_2 increases the NO conversion. The N850A400 catalyst shows over 90 % NO conversion at 170 - 430 °C. In terms of cost and energy consumption, stabilization temperature above 850 °C do not be advocated in the present study.

We further studied the effect of removing of carbon template with different annealing temperatures in air on SCR activity over Ce-Ti-MoO_x catalyst. The result

indicates that the annealing temperature in air influences the SCR activity significantly. From **Fig. 1(b)**, the NO conversions on the Ce-Ti-MoO_x catalysts decrease with the increase of annealing temperature for removing of carbon template in air. The highest NO conversion over N550A850 catalyst is only 50 %, which indicates the higher calcination temperature for removing of carbon template can lead to an abrupt deactivation of Ce-Ti- MoO_x catalysts.

The results of the N_2 selectivity and the production of N_2O are shown in **Fig. 2**. It can be inferred from **Fig. 2** that all the Ce-Ti-MoO_x catalysts exhibit over 95% of N_2 selectivity and no more than 25 ppm of N_2O concentration at 150-350 °C except for N550A850. The N850A400 catalyst even shows over 98% of N_2 selectivity and no more than 12 ppm of N_2O concentration at 150-350 °C. Although the Ce-Ti-MoO_x catalysts present inferior N_2 selectivity above 375 °C, generally, the typical temperatures of diesel exhaust operate at 150-250 °C for light duty and 200-350 °C for heavy duty diesel engines.[5, 6] So the N_2 selectivity of Ce-Ti-MoO_x catalyst can match well with the operating temperature of light and heavy duty diesel exhausts, indicating the application potential of the Ce-Ti-MoO_x catalysts.

3.2 XRD analysis

Fig. 3(a) shows the XRD patterns of pure CeO_2, MoO_3 and TiO_2. The result indicates that all the pure samples present intense and sharp diffraction peaks. For pure CeO_2, MoO_3 and TiO_2, crystalline phases of cerianite CeO_2, orthorhombic MoO_3 and anatase TiO_2 are observed, respectively. The XRD patterns of the Ce-Ti-MoO_x with different treating conditions are shown in **Fig. 3(b) and (c)**. As shown in **Fig. 3(b)**, the Ce-Ti-MoO_x catalyst with different stabilization temperatures in the presence of carbon template in N_2 atmosphere shows no obvious diffraction peaks of any molybdenum and titanium oxides. Furthermore, no obvious diffraction peaks of any cerium oxides are observed until the stabilization temperature is 850 °C, but N850A400 only shows slight diffraction peaks of cerianite CeO_2.

The X-ray powder diffraction (XRD) patterns of the Ce-Ti-MoO_x catalysts treating with different temperatures in air for removing of carbon template are shown in **Fig.3 (c)**. The result indicates that the calcination temperature in air influences the

crystalline phases significantly. The XRD pattern of Ce-Ti-MoO_x catalyst treating at 450 °C in air shows no visible phase of Ce, Mo or Ti. But when the annealing temperature in the air is beyond 550 °C, the Ce-Ti-MoO_x catalyst exhibits an increasingly intense and sharp peak of cerianite CeO_2. The Diffraction peaks of monoclinic MoO_2 phase appear when the calcination temperature at 550 - 650 °C. However, when the calcination temperature is up to 750 °C, the diffraction peaks of monoclinic MoO_2 disappear. When Ce-Ti-MoO_x catalyst is calcined at 750 - 850 °C in air, the obvious phase of rutile TiO_2 can be detected.

It is clear that the Ce-Ti-MoO_x catalyst stabilization with carbon template can inhibit the generation of rutile TiO_2 under thermal-treating temperature as high as 850 °C. Otherwise, the Ce-Ti-MoO_x catalyst stabilization with carbon template in N_2 lead to the absence of molybdenum, titanium and CeO_2 crystallization phases, which indicates strong interactions exist among molybdenum, titanium and cerium oxides. The Ce-Ti-MoO_x catalyst treating with an increasing temperature in air for removing of carbon template leads to an increase of crystallization of metal oxide. As a result, the enhanced crystallization of metal oxide reduces the interactions among metal oxides.

3.3 N_2 adsorption-desorption results

The specific surface area (*SSA*), pore volume and pore size of various catalysts are listed in **Table 1**. For Ce-Ti-MoO_x catalyst, the increase of stabilization temperature in the presence of carbon template in N_2 atmosphere leads to an increasing trend of surface areas and cumulative pore volumes. But the Ce-Ti-MoO_x catalyst treating with an increasing temperature in air for removing of carbon template leads to a sharp decrease of surface areas and cumulative pore volumes. It could be seen from **Table 1** that N850A400 exhibits the largest specific surface area (91 m^2/g) and cumulative pore volumes (0.106 cm^3/g), while N550A850 shows the least specific surface area of 1 m^2/g and cumulative pore volumes of 0.003. Therefore, it could be concluded that the stabilization treating in the presence of carbon template can prevent Ce-Ti-MoO_x catalyst from being sintered under the thermal-treating temperature as high as 850 °C.

The nitrogen sorption isotherms of the Ce-Ti-MoO_x catalysts with different

stabilization temperatures in the presence of carbon template in N_2 atmosphere are listed in **Fig. 4(a)**. It can be inferred from **Fig.4(a)** that the isotherms of Ce-Ti-MoO_x catalysts exhibit a typical shape of type IV (IUPAC classification), indicating the presence of mesorpores (2-50 nm).[27] The narrow hysteresis loops of catalysts listed in **Fig.4(a)** exhibited a typical type H2 (IUPAC classification), indicating a narrow distribution of pore diameters.[28] The nitrogen sorption isotherms of the Ce-Ti-MoO_x catalysts with different annealing temperatures in air for removing of carbon template are listed in **Fig.4 (b)**. The nitrogen sorption isotherms of N450A450, N550A550 and N550A650, can also be assign to the typical shape of type IV (IUPAC classification), indicating the presence of mesorpores. Isotherms of N450A450 and N550A550 show an uptake at a low relative pressure ($P/P_0 \leq 0.03$), indicating the presence of micropores,[29] while the hysteresis loops of N550A550 and N550A650 approach $P/P_0=1$, indicating the presence of macrospores (＞50 nm). Thus, it could be inferred that pore size distributions of N550A550 and N550A650 is wider than that of N450A450. N550A750 and N550A850 exhibit a typical shape of type III (IUPAC classification), indicating the non-porous structures.

The pore size distributions calculated from N_2 adsorption isotherms of various Ce-Ti-MoO_x catalysts are shown in **Fig. 5**. It can be seen from **Fig. 5** that the Ce-Ti-MoO_x catalysts treating with different stabilization temperature in the presence of carbon template in N_2 atmosphere exhibit a narrow pore size distributions in the main range of 2-12 nm. The full width at half maxima (fwhm) of below 4 Å measured for the pore-size distribution in the main range of 2-10nm for N750A400 and N850A400 indicate the uniform mesoporous dimensions. N850A400, which contains the largest pore volume and S_{BET} exhibit higher NH_3-SCR activity than the others. N650A400 and N550A400, which exhibit a wider pore size distribution at 2-10 nm and no more than 4 nm of fwhms, also reflects the uniform mesoporous distributions. The N450N400 reflects the multimodal pore size distribution in the range of 2-12 nm. In comparison, it can be seen from **Fig. 5** that N550A550 and N550A650 exhibit a broad diameter range of pore size distribution. Above all, the Ce-Ti-MoO_x catalyst with the increase of stabilization temperature in the presence of carbon template in N_2

atmosphere may attribute to the decreasing diameter range of pore size distributions. In contrast, ranges of pore size distributions can be extended by increasing treating temperatures at 450-650 °C in air for removing of carbon template. Ce-Ti-MoO_x catalysts calcining above 650 °C in air for removing of carbon template may lead to the collapse of pore structure. To our great interests, it can be inferred that narrow diameter range of pore size distributions is proffered to improve low-temperature NO conversion over Ce-Ti-MoO_x catalysts as described in **Fig.1**.

3.4 HR-TEM analysis

High-resolution transmission electron microscopy (HR-TEM) analysis is used to further explore the phase composition, microstructure and the particle size distribution of the catalysts. Metal oxide crystals are determined by the interplanar distance measurement. It can be obviously seen from **Fig. 6(c)** and **Fig. 6(d)** that the N850A400 catalysts has a mean particle diameter of ~22 nm (range from 9 to 27 nm), while the N550A850 catalysts has a mean particle diameter of ~282 nm (range from 165 to 356 nm). Therefore, it is evident that the stabilization treating in the presence of carbon template in N_2 atmosphere is rather critical to stop the Ce-Ti-MoO_x catalysts from being sintered. Lattice fringes of N850A400 (**Fig. 6(a)**) with an interplanar distance of 0.271 nm reveal the (200) lattice plane of the cubic cerianite cell,[30] indicating the existence of cerianite CeO_2 structure. In addition, it is can be seen from **Fig. 6(a)** that N850A400 show no more than 10 nm of cerianite crystallite size. Over half of the areas adjacent to the cerianite CeO_2 (**Fig. 6(a)**) could be attributed to semi-crystalline or amorphous zone of non-crystalline molybdenum, titanium and cerium oxides. Lattice fringes of anatase, rutile as well as MoO_3 could not be observed from the image of N850A400, in consistent with our XRD results, indicating high dispersions of amorphous metal oxides and strong interactions among tri-metal oxides. In comparison, it can be seen from HR-TEM images of N850A400 in **Fig. 6(c)** that lattice fringes with interplanar distance of 0.314 nm and 0.324nm are correspond to crystallite orientations of cerianite CeO_2 (111) [30-32] and rutile TiO_2 (110) [33, 34] respectively. It is noteworthy that rutile TiO_2 and cerianite CeO_2 crystals of N550A850 has a crystallite size of more than 20nm (**Fig. 6(c)**), indicating the high

crystallinity of cerium and titanium oxides, while lattice fringes of anatase TiO_2 and MoO_3 could not be observed. Thus, it can be inferred that a majority of molybdenum existed in the forms of surface amorphous species, while a majority of surface titanium and cerium oxides are transformed to bulk TiO_2 and CeO_2 as the calcination of Ce-Ti-MoO_x at 850 °C in air for removing of carbon template. To our best knowledge, the decrease of surface amorphous titanium and cerium oxides may lead to a relative increase of surface molybdenum species and decrease of interactions among amorphous surface molybdenum, titanium and cerium oxides. Hence, further study of temperature programmed reduction and surface analysis are expected to explore and interaction among the tri-metal oxides.

3.5 H_2-TPR and XPS results

3.5.1 H_2-TPR results

Redox properties of cerium-based catalysts is rather critical for oxygen storage capacity (OSC) in standard NH_3-SCR process ($4NH_3 + 4NO + O_2 \rightarrow 4N_2 + 4H_2O$) in the presence of excess oxygen since NO consists > 90% of NO_x in diesel exhausts.[9] Thus, H_2-TPR is a useful tool in evaluating redox properties of the SCR catalyst. **Fig. 7** presents the H_2-TPR profiles of various catalysts. A gradual consumption of H_2 at 260 to 532 °C could be assigned to the removal of surface oxygen-containing functional groups,[35] partial reduction of surface $Ce^{4+} \rightarrow Ce^{3+}$,[36-38] and well-dispersed high-valent Mo (VI) species.[39, 40] It is well-known that reduction of titanium oxides is harder than that of cerium and molybdenum oxides below 700 °C,[36, 41] therefore, peaks of various catalysts listed below 700 °C could be assigned to the reduction of surface CeO_2 and reduction of Mo (VI) to Mo (IV). It is well known that the relative amount of reducible components can be assessed by H_2 consumption of H_2-TPR. The total H_2 consumption over different catalyst at 400-800 °C are calculated and listed in Table 2. As shown in Table 2, the H_2 consumptions of various catalysts are in an order of N850A400 > N750A400 > N550A750 > N550A850, respectively. It also can be seen from **Fig. 7** that the reduction peak of N850A400 exhibits a higher intensity of H_2 consumption and a lower reduction temperature than the others listed, indicating the highest oxygen-storage capacity of N850A400. In terms of N850A400 and

N750A400, it could be inferred that the Ce-Ti-MoO_x with higher stabilization temperature in the presence of carbon template in N_2 atmosphere is preferred to enhance the redox capacity. Reduction peaks of N550A750 and N550A850 shift to 673 °C, obviously higher than the others, indicating the decrease of interaction among metal oxides species and/or the drastic decrease of well-dispersed surface metal oxides during the calcination process in air for removal of carbon template, in consistent with our XRD (**Fig. 3(c)**) and HR-TEM (**Fig. 6(c)** and **(d)**) results. It is noteworthy that N550A850 exhibits a lower intensity of H_2 consumption than that of N550A750 at 650 to 775 °C, indicating the sharp decrease of amorphous surface molybdenum and/or cerium oxides. However, in order to determine this decrease of the reduced surface species, further study of surface composition, chemical states of metal species are still expected.

3.5.2 XPS analysis results

X-ray photoelectron spectroscopy (XPS) analysis is used to clarify surface composition and chemical states of the catalysts. Surface atomic concentrations of Ce, Ti, Mo and O are determined. While the peak areas and the full widths at half maximas (fwhms) are determined by using XPS PeakFit (Version 4.0, AISN Software Inc.) program. To our present studies, surface atomic ratios of Ce^{3+}/Ce^{4+} according to the following equation

$$\mathrm{Ce}^{3+}(\%) = \frac{S_2 + S_6}{S_1 + S_2 + S_3 + S_4 + S_5 + S_6 + S_7 + S_8} \tag{3}$$

S_1, S_2, S_3, S_4, S_4, S_5, S_6, and S_7 represent the peak areas of corresponding u, u′, u′′, u′′′, v, v′, v′′ and v′′′ lines, respectively.

Surface atomic ratios of $O_{surface}/O_{total}$ are determined according to the following equation

$$\mathrm{O_{surface}/O_{total}}(\%) = \frac{S_{surface}}{S_{surface} + S_{lattice}} \times 100\% \tag{4}$$

Where $S_{surface}$ and $S_{lattice}$ are the peak areas corresponding to O^{2-} and OH^-/CO_3^{2-} respectively.

Table 3 shows binding energy and full width at half maxima (fwhm) of surface

titanium species of N850A400 and N550A850 determined from XPS analysis. Two peaks of Ti 2p orbital located at around 458.5 and 464.3 eV indicate titanium species N850A400 and N550A850 exist in the forms of titanium (IV) species. N550A850 shows smaller full width at half maxima (fwhm) than that of N850A400 indicates that N550A850 has a higher degree of order.[42, 43] While high degree of order may further indicate high crystallinity of surface titanium species,[44] in consistent with our XRD (**Fig. 3(b)** and **(c)**) and HR-TEM (**Fig. 6(a)** and **(c)**) analysis results. Therefore, it can be concluded that the different stabilization temperatures in the presence of carbon template in N_2 atmosphere and the different calcination temperatures for removal of carbon template have little effect on valence states of titanium (IV) species.[44, 45] It could be seen from **Fig. 8(a)** and **Fig. 8(b)** that obvious peaks and shoulders located at 529.2-530.3 and 530.4-531.2 could be attributed to lattice oxygen (O^{2-}), hydroxyl and/or carbonate species and adsorbed oxygen respectively.[46, 47] No obvious signals of surface adsorbed molecular water could be detected.

Ce 3d XPS spectra are listed in **Fig. 9(a)** and **Fig. 9(b)**. The peaks located at 883.2 ± 0.2 eV, 889.3 ± 0.4 eV, 899.0 ± 0.3 eV (denoted with u, u´´ and u´´´ respectively) represent the spin-orbita doublets of Ce $3d_{5/2}$ and peaks located 901.8 ± 0.3 eV, 908.3 ± 0.3eV and 917.3 ± 0.3 (denoted with v, v´´ and v´´´ respectively) represent the Ce 3 $d_{3/2}$, indicating the presence of Ce^{4+}. The shoulders located at 886.0 ± 0.3 eV and 904.1 ± 0.4 eV (denoted with u´ and v´ respectively) could be assigned to Ce^{3+}.[31, 48] The peaks of u, u´´ and u´´´ represent the Ce $3d_{5/2}$ could be attributed to the multielectron configuration of $3d^94f^2$ (O $2p^4$), $3d^94f^1$ (O $2p^5$) Ce^{4+} and $3d^94f^0$ (O $2p^6$) Ce^{4+} final state, while the shoulder u´ located at 886.0 ± 0.3 eV could be attributed to the multielectron configuration of $3d^94f^1$ (O $2p^6$) Ce^{3+} final state.[49-52] Thus, it can be concluded that a majority of surface cerium species is Ce^{4+}, while Ce^{3+} oxidation state is indistinctly identified through the Ce 3d spectra. XPS spectrums of Mo 3d for various catalysts are listed in **Fig. 10(a)** and **Fig. 10(b)**. All the spectrums contained duplet signals corresponding to Mo (VI) oxide with a binding energy of ~ 232.5 eV, correspond to binding energy of Mo $3d_{3/2}$, indicating the presence of Mo^{6+} surface species.[53] Combining with our HR-TEM and XRD analysis, it could be

concluded that Mo existed in the forms of amorphous Mo^{6+} and Mo^{n+} (0< n <6) species.[53]

To our best knowledge, the presence of surface OH groups may facilitate NO adsorption in the presence of oxygen,[54] surface adsorbed H_2O and OH groups may play an important role on adsorption activation of NH_3 in NH_3-SCR process.[55] In addition, a proper surface molar ratios of Ce^{3+}/Ce^{4+} plays an important role in $Ce^{3+} \rightleftharpoons Ce^{4+}$ redox cycle for NH_3-SCR process in the presence of oxygen.[10] It can be seen from **Table 4** that the surface cerium, titanium, molybdenum, oxygen atomic concentration, $O_{surface}/O_{total}$ and Ce^{3+}/Ce^{4+} of all Ce-Ti-MoO_x catalysts listed show no obvious differences of within systematic errors except for N550A850, which shows an drastic decrease of $O_{surface}/O_{total}$, surface cerium concentration and an abrupt increase of surface molybdenum, titanium and oxygen concentration. Thus, it can be inferred that a shift of calcination temperature for removal of carbon template in air from 750 to 850 °C may lead to an abrupt increase of surface titanium, molybdenum and oxygen atomic concentration as well as an abrupt decrease of $O_{surface}/O_{total}$, in consistent with our H_2-TPR analysis. It is interesting that N550A750 and N550A850 show no significant difference in *SSA*, pore size properties and phase compositions, while N550A850 shows an abrupt decrease of NO_x conversion as described in **Fig. 1(b)**. Therefore, it could be inferred that different surface atomic ratios might be one of the major part that attribute to significant difference of NH_3-SCR activity.

4. Conclusion

The present work has successfully synthesized a mesoporous Ce-Ti-MoO_x catalyst stabilized by the in-situ formed carbon template. The higher stabilization temperature in the presence of carbon template in N_2 atmosphere and the lower thermal-treating temperature for removal of carbon template have promoted influence on NO reduction activity. The Ce-Ti-MoO_x catalyst stabilized with carbon template at 850 °C in N_2 atmosphere and calcined at 400 °C in air for removal of carbon template exhibits nano particle size of 22 nm, largest surface area of 91 m^2/g and highest SCR

activity at 150 - 450 °C. The higher the stabilization temperature in the presence of carbon template in N_2 atmosphere, the higher surface areas and low-temperature NO conversions are obtained. The stabilization treating with carbon template in N_2 can stop the crystallization of molybdenum, titanium and cerium oxides. The higher the thermal-treating temperature for removal of carbon template, the lower surface areas and NO conversions are gained. Otherwise, the increasing calcination temperature for removal of carbon template contributes to increased crystallinity of titanium and increasing collapse of pore structures.

Acknowledgements

This work is supported by the National Natural Science Foundation of China (No. U1137603, No. 21307047) and the Opening Project of Key Laboratory of Green Catalysis of Sichuan Institutes of High Education (LYJ1309).

References

[1] S. Brandenberger, O. Kröcher, A. Tissler and R. Althoff, *Catal. Rev*., 2008, **50**, 492-531.

[2] R. Q. Long and R. T. Yang, *J. Catal*., 1999, **188**, 332-339.

[3] H. Huang, W. Shan, S. Yang and J. Zhang, *Catal. Sci. Technol*., 2014, **4**, 3611-3614.

[4] J. Li, H. Chang, L. Ma, J. Hao and R. T. Yang, *Catal. Today*, 2011, **175**,147-156.

[5] Y. J. Kim, H. J. Kwon, I. Heo, I. S. Nam, B. K. Cho, J. W. Choung, M. S. Cha and G. K. Yeo, *Appl. Catal., B,* 2012, **126**, 9-21.

[6] D. S. Kim and C. S. Lee, *Fuel*, 2006, **85**, 695-704.

[7] B. Thirupathi and P. G. Smirniotis, *Appl. Catal., B*, 2011, **110**, 195-206.

[8] J. Li, J. Hao, L. Fu, Z. Liu and X. Cui, *Catal. Today*, 2004, **90**, 215-221.

[9] M. Koebel, M. Elsener and M. Kleemann, *Catal. Today*, 2000, **59**, 335-345.

[10] Y. Peng, K. Li and J. Li, *Appl. Catal., B*, 2013, **140-141**, 483-492.

[11] Z. Yan, J. Fan, Z. Zuo, Z. Li and J. Zhan, *Appl. Surf. Sci*., 2014, **288**, 690-694.

[12] H. L. Koh and H. K. Park, *J. Ind. Eng. Chem*., 2013, **19**, 73-79.

[13] X. Gao, Y. Jiang, Y. Zhong, Z. Y. Luo and K. F. Cen, *J. Hazard. Mater*, 2010, **174**, 734-739

[14] X. Gao, Y. Jiang, Y. Zhong, Z. Y. Luo and K. F. Cen, *Catal. Commun*., 2010, **11**, 465-469.

[15] L. Chen, J. H. Li and M. F. Ge, *J. Phys. Chem., C*, 2009, **113**, 21177-21184

[16] F. D. Liu, Y. B. Yu and H. He, *Chem. Commun*., 2014, **50**, 8445-8463

[17] Q. L. Zhang, Z. X. Song, P. Ning, X. Liu, H. Li and J. J. Gu, *Catal. Commun*., 2015, **59**, 170-174

[18] Z. C. Si, D. Weng, X. D. Wu, J. Yang and B. Wang, *Catal. Commun*., 2010, **11**, 1045-1048

[19] C. X. Liu, L. Chen, H. Z Chang, L. Ma, Y. Peng, H. Arandiyan and J. H. Li, *Catal. Comm*., 2013, **40**, 145-148

[20] W. P. Shan, F. D. Liu, H. He, X. Y. Shi and C. B. Zhang, *Chem. Commun*., 2011, **47**, 8046-8048

[21] X. L. Li and Y. H. Li, *Catal. Lett*., 2014, **144**:165-171.

[22] Z. Liu, J. Zhu, S. Zhang, L. Ma and S. I. Woo, *Catal. Commun*., 2014, **46**, 90-93.

[23] Z. Liu, S. Zhang, J. Li and L. Ma, *Appl. Catal., B*, 2014, **144**, 90-95.

[24] A. Corma, Chem. Rev., 1997, **97**, 2373-2420.

[25] M. F. Luo, Y. P. Song, X. Y. Wang, G. Q. Xie, Z. Y. Pu, P. Fang and Y. L. Xie, *Catal. Commun*., 2007, **8**, 834-838.

[26] L. Chen, X. Sun, Y. Liu and Y. Li, *Appl. Catal., A*, 2004, **265**, 123-128.

[27] H. Imagawa and S. Sun, *J. Phys. Chem., C*, 2011, **115**, 22901-22909.

[28] H. Imagawa and S. Sun, *J. Phys. Chem., C*, 2012, **116**, 2761-2765.

[29] S. Chin, E. Park, M. Kim, J. Jeong, G. N. Bae and J. Jurng, *Powder Technol*., 2011, **206**, 306-311.

[30] Y. Y. Lv, X. F. Qian, B. Tu and D. Y. Zhao, *Catal. Today*, 2013 **204**, 2-7.

[31] M. S. P. Francisco, V. R. Mastelaro, P. A. P. Nascente and A. O. Florentino, *J. Phys. Chem., B*, 2001, **105**, 10515-10522.

[32] M. Han, X. Wang, Y. Shen, C. Tang, G. S Li and R. L. Smith, Jr., *J. Phys. Chem., C*, 2010, **114**, 793-798.

[33] J. Li, R. Büchel, M. Isobe, T. Mori and T. Ishigaki, *J. Phys. Chem., C*, 2009, **113**, 8009-8015.

[34] M. Andersson, A. Kiselev, L. Österlund and A. E. C. Palmqvist, *J. Phys. Chem., C*, 2007, **111**, 6789-6797.

[35] M. E. Pirez, P. Granger and G. Leclercq, *Catal. Today*, 2005, **107-108**, 315-322.

[36] S. N. R. Inturi, T. Boningari, M. Suidan and P. G. Smirniotis, *Appl. Catal., B*, 2014, **144**, 333-342.

[37] A. Trovarelli, G. Dolcetti, C. de Leitenburg, J. Kašpar, P. Finetti and A. Santoni, *J. Chem. Soc. Faraday Trans*., 1992, **88**, 1311-1319.

[38] H. Chen, A. Sayari, A. Adnot and F. Larachi, *Appl. Catal., B*, 2001, **32**, 195-204.

[39] P. Arnoldy, J. C. M. de Jonge and J. A. Moulijn, *J. Phys. Chem*., 1985, **89**, 4517-4526.

[40] L. C. Caero, A. R. Romero and J. Ramirez, *Catal. Today*, 2003, **78**, 513-518.

[41] M. Luo, J. Chen, L. Chen, J. Lu, Z. Feng and C. Li, *Chem. Mater*., 2001, **13**, 197-202.

[42] Z. He, W. Que, J. Chen, Y. He and G. Wang, *J. Phys. Chem. Solids*, 2013, **74**, 924-928.

[43] B. M. Reddy, B. Chowdhury, E. P. Reddy and A. Fernández, *Appl. Catal., A*, 2001, **213**, 279-288.

[44] B. Guan, H. Lin, L. Zhu and Z. Huang, *J. Phys. Chem., C*, 2011, **115**, 12850-12863.

[45] S. Södergren, H. Siegbahn, H. Rensmo, H. Lindström, A. Hagfeldt and S. E. Lindquist, *J. Phys. Chem., B*, 1997, **101**, 3087-3090.

[46] S. Ponce, M. A. Peña and J. L. G. Fierro, *Appl. Catal., B*, 2000, **24**, 193-205.

[47] H. Najjar, J. F. Lamonier, O. Mentre, J. M. Giraudon and H. Batis, *Appl. Catal., B*, 2011, **106**, 149-159.

[48] R. Gao, D. Zhang, P. Maitarad, L. Shi, T. Rungrotmongkol, H. Li, J. Zhang and W. Cao, *J. Phys. Chem., C*, 2013, **117**, 10502-10511.

[49] P. O. Larsson and A. Anderssony, *J. Catal*., 1998, **179**, 72-89.

[50] B. Ernst, L. Hilaire and A. Kiennemann, *Catal. Today*, 1999, **50**, 413-427.

[51] N. Thromat, M. Gautier-Soyer and G. Bordier, *Surf. Sci*., 1996, **345**, 290-302.

[52] F. Le Normand, L. Hilaire, K. Kili, G. Krill and G. Maire, *J. Phys. Chem*., 1988, **92** , 2561-2568.

[53] P. A. Zosimova, A. V. Smirnov, S. N. Nesterenko, V. V. Yuschenko, W. Sinkler, J. Kocal, J. Holmgren and I. I. Ivanova, *J. Phys. Chem., C*, 2007, **111**, 14790-14798 .

[54] J. C. S. Wu and Y .T. Cheng, *J. Catal*., 2006, **237**, 393-404.

[55] W. Shan, F. Liu, H. He, X. Shi and C. Zhang, *Appl. Catal., B*, 2012, **115-116**, 100-106.

Figure Captions:

Fig. 1. NH_3-SCR activities over Ce-Ti-MoO_x catalysts. Reaction conditions: [NO] = [NH_3] = 600 ppm, [O_2] = 5%, N_2 balanced, GHSV = 60 000h^{-1}.

Fig. 2. N_2 selectivity and N_2O concentration over different catalysts. Reaction conditions: [NO] = [NH_3] = 600 ppm, [O_2] = 5%, N_2 balanced, GHSV = 60 000h^{-1}.

Fig. 3. XRD patterns of (a) pure CeO_2, TiO_2 and MoO_3, (b) and (c) Ce-Ti-MoO_x catalysts with different treating conditions.

Fig. 4. N_2 adsorption-desorption isotherms of various catalysts at 77 K.

Fig. 5. Pore size distributions of different Ce-Ti-MoO_x catalysts

Fig. 6. High-resolution transmission electron microscopy (HR-TEM) of (a) and (b), and (c) and (d) N850A400 catalysts.

Fig. 7. H_2-TPR profiles of various catalysts.

Fig. 8. XPS patterns of O 1s spectra over Ce-Ti-MoO_x catalysts.

Fig. 9. XPS patterns of Ce 3d spectra : (1) N450A400, (2) N550A400, (3) N650A400, (4) N750A400, (5) N850A400, (6) N450A450, (7) N550A550, (8) N550A650, (9) N550A750 and N550A850

Fig. 10. XPS patterns of Mo 3d spectra over Ce-Ti-MoO_x catalysts.

Table Captions:

Table 1 BET specific surface area, pore volume and pore size of various catalysts

Table 2 H_2 consumption of various catalysts

Table 3 Fwhm of surface titanium species determined from XPS analysis

Table 4 Surface atomic concentration of the Ce-Ti-MoO_x catalysts determined by the XPS analysis.

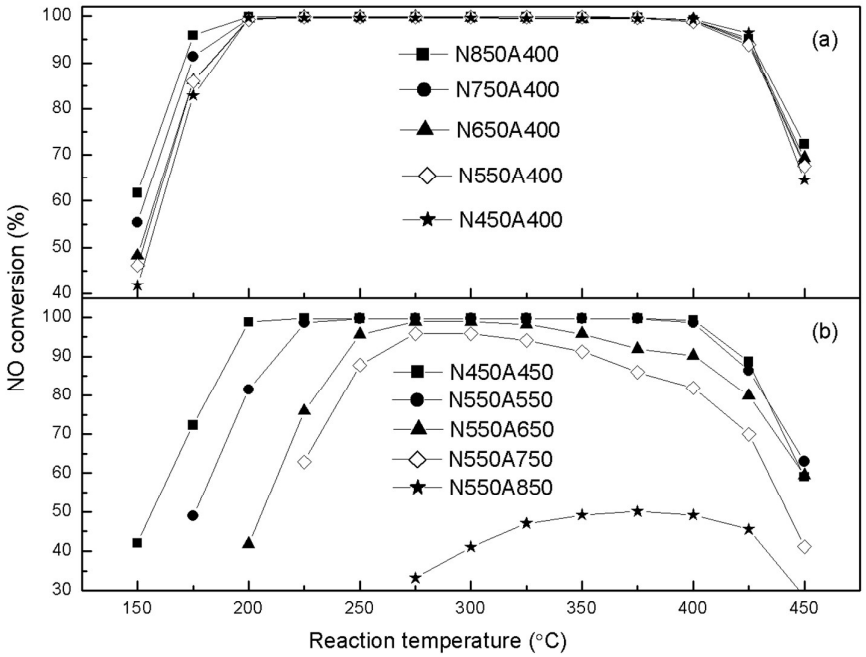

Fig. 1

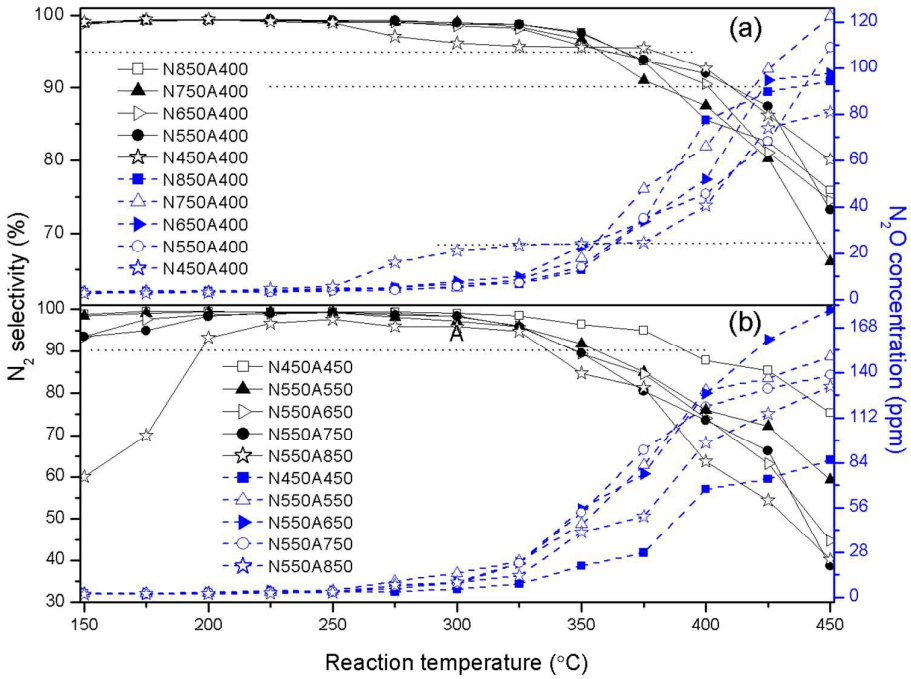

Fig. 2

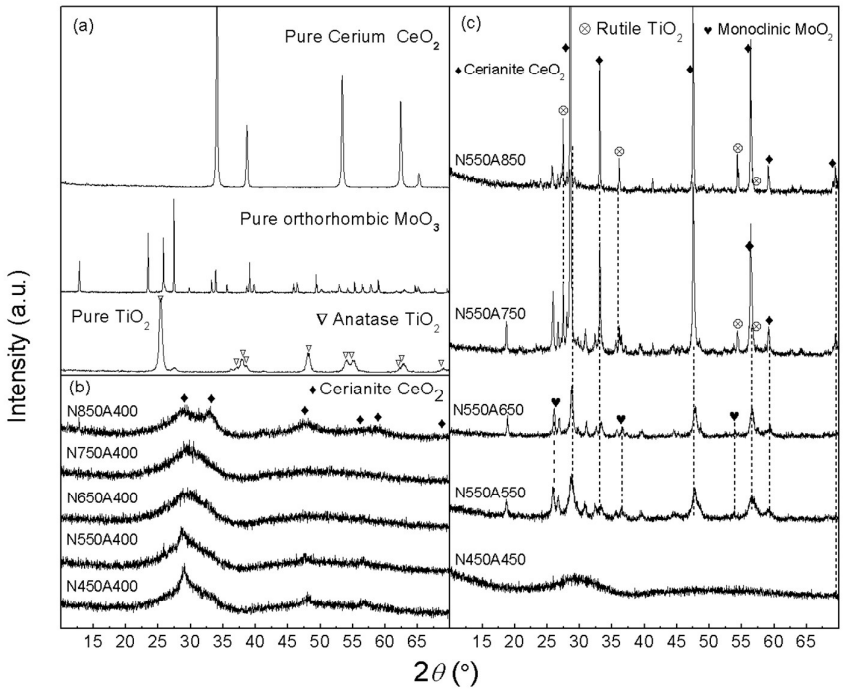

Fig. 3

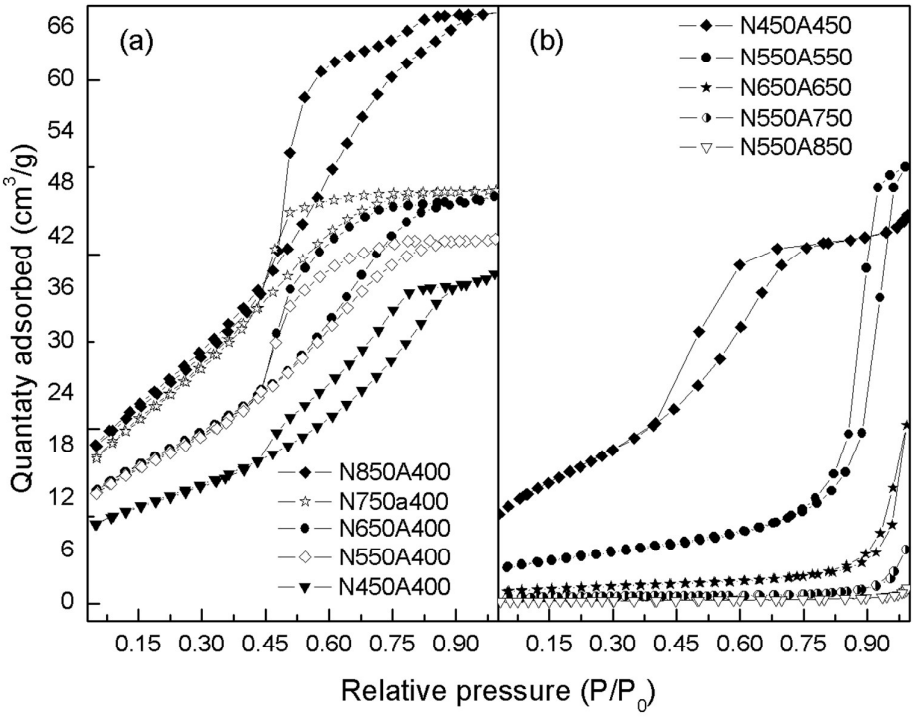

Fig. 4

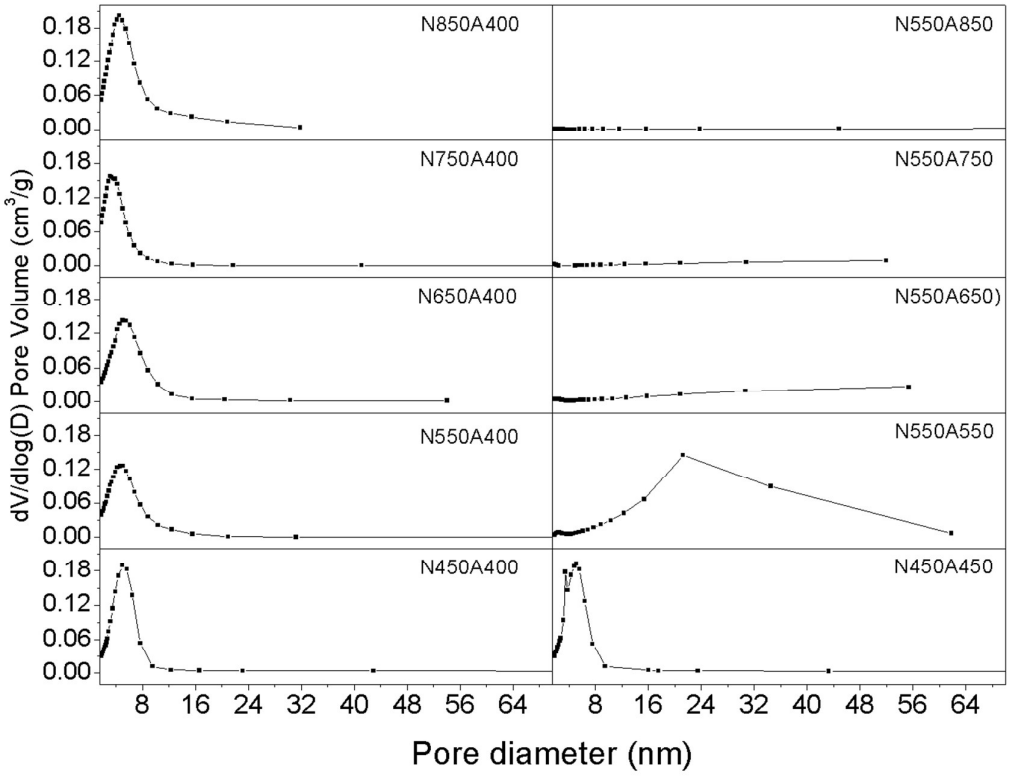

Fig. 5

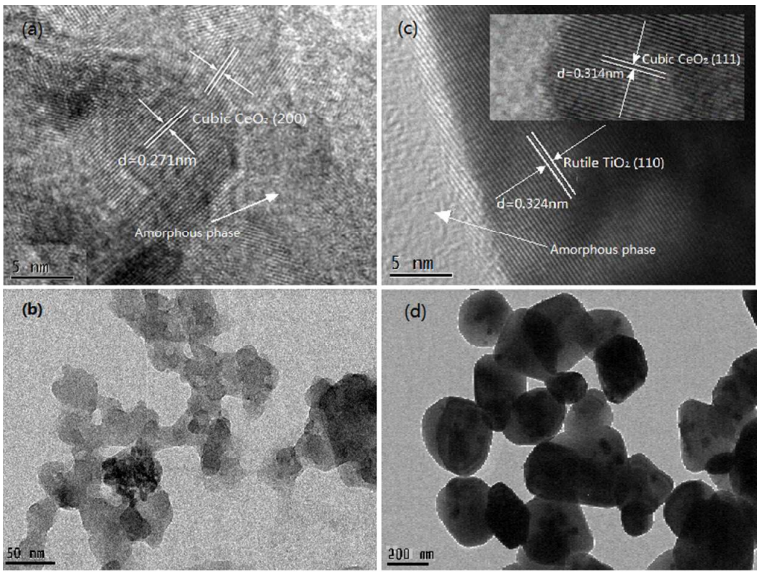

Fig. 6

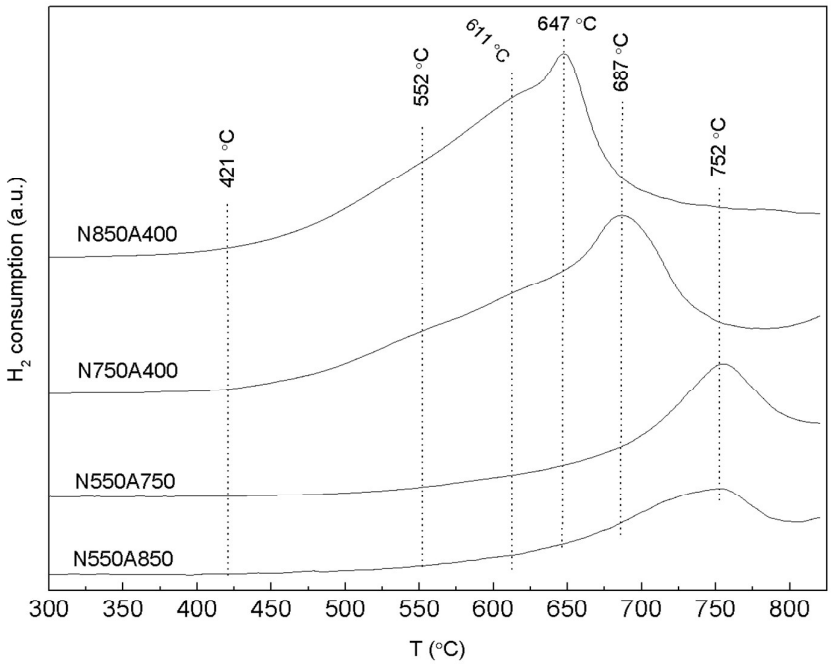

Fig. 7

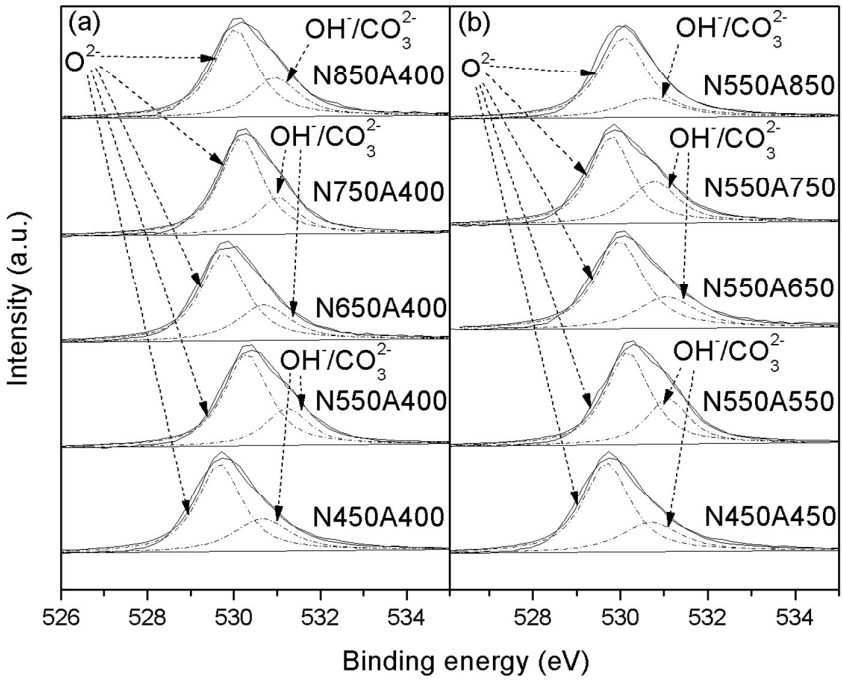

Fig. 8

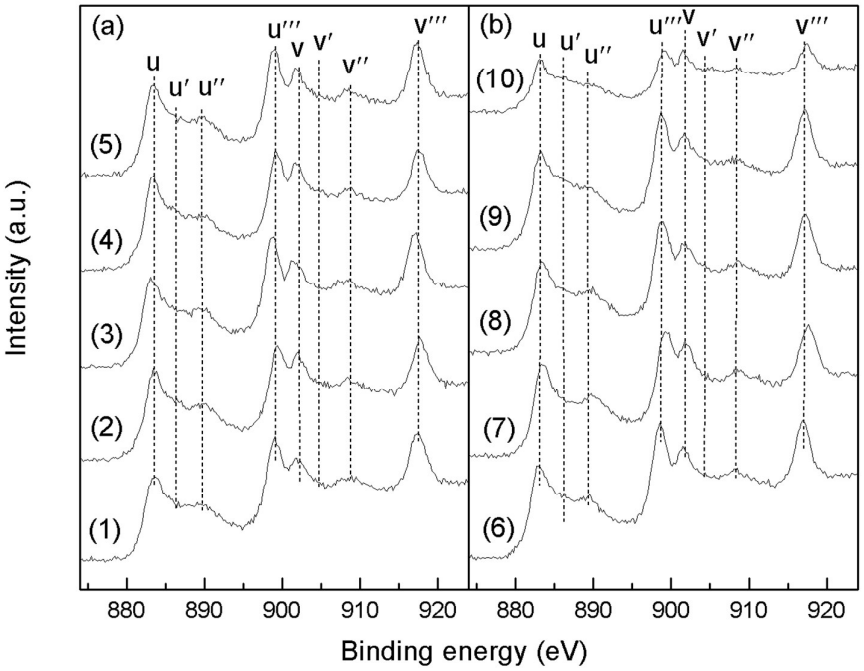

Fig. 9

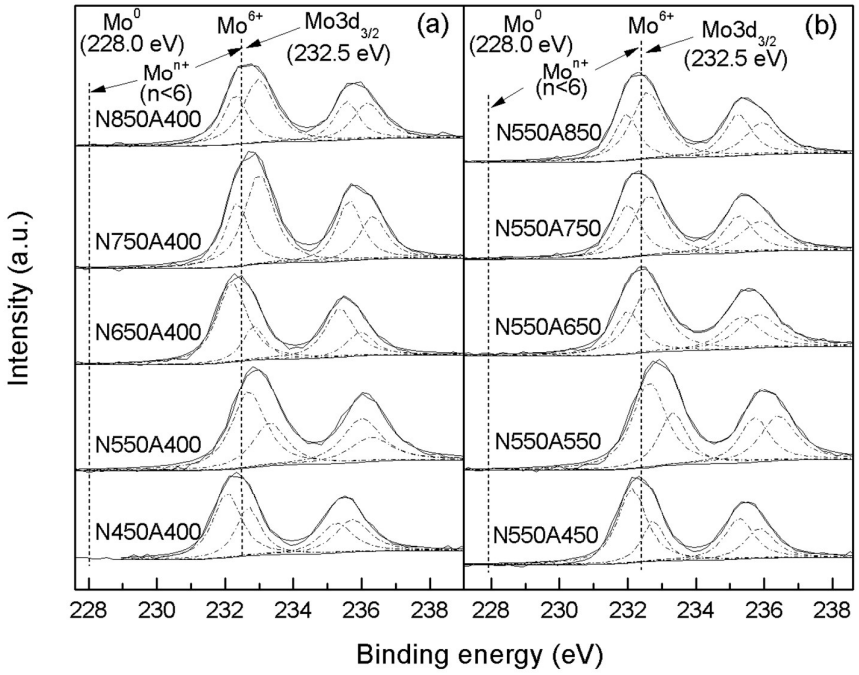

Fig. 10

Table 1

Samples	SSA (m^2/g)	Pore volume (cm^3/g)
N450A400	42	0.060
N550A400	60	0.066
N650A400	62	0.074
N750A400	86	0.074
N850A400	91	0.106
N450A450	55	0.084
N550A550	19	0.077
N550A650	6	0.032
N550A750	3	0.009
N550A850	1	0.003

Table 2

Samples	N850A400	N750A400	N550A750	N550A850
Areas (a.u.)	8296	7256	37476	3172

Table 3

Samples	Positions (eV)		Fwhms (eV)	
	2p 3/2	2p1/2	2p 3/2	2p1/2
N850A400	458.6	464.4	1.43	2.13
N550A850	458.7	464.5	1.13	1.92

Table 4

Samples	Surface atomic concentration (%)						
	Ce	Ti	Mo	O	$O_{surface}/O_{total}$	Ce^{3+}/Ce^{4+}	Ce: Ti: Mo
N450A400	37.03	9.45	3.93	49.58	0.314	0.148	1: 0.25: 0.11
N550A400	35.32	9.27	5.40	50.01	0.281	0.157	1: 0.26: 0.15
N650A400	37.65	9.24	4.30	48.81	0.317	0.164	1: 0.25: 0.11
N750A400	36.57	8.61	5.67	49.15	0.266	0.158	1: 0.24: 0.16
N850A400	36.43	9.92	4.10	49.55	0.321	0.143	1: 0.27: 0.11
N450A450	36.27	8.71	4.17	50.85	0.294	0.161	1: 0.24: 0.11
N550A550	35.76	9.66	4.90	49.68	0.317	0.191	1: 0.27: 0.14
N550A650	37.32	9.64	3.96	49.08	0.302	0.164	1: 0.26: 0.11
N550A750	39.20	8.75	3.84	48.2	0.346	0.191	1: 0.22: 0.10
N550A850	24.02	14.06	6.65	55.27	0.231	0.186	1: 0.58: 0.28